CHINESE JOURNAL OF GEOPHYSICS Vol.55, No.3, 2012, pp: 359∼374

RELATIONSHIP AND MECHANISM BETWEEN PERTURBATION POTENTIAL ENERGY AND ATMOSPHERIC GENERAL CIRCULATION ANOMALIES

GAO Li[1], LI Jian-Ping[2]

1 *Numerical Prediction Center, National Meteorological Center, China Meteorological Administration, Beijing* 100081*, China*

2 *State Key Laboratory of Numerical Modeling for Atmospheric Sciences and Geophysical Fluid Dynamics, Institute of Atmospheric Physics, Chinese Academy of Sciences, Beijing* 100029*, China*

Abstract Based on previous theoretical studies for local perturbation potential energy (PPE), in this study, we further focus on the relationship and mechanism between the PPE and atmospheric general circulation anomalies, and analyze coupled correlation modes between the PPE and upper, middle and lower-level atmospheric kinetic energy (AKE) and their interannual variability. Meanwhile, we also examine the relationship between the PPE and sea surface pressure as the measure of atmospheric mass and further discuss the physical mechanisms involved in the relationships between the PPE and the AKE as well as mass. Analysis results show that the first mode in the variability of the PPE is also the leading mode in the coupled variation of the PPE and atmospheric general circulation anomalies, and the corresponding primary modes in the AKE and mass fields are also the dominant modes in their own variability, which indicates a possible interrelated physical mechanism between them. Furthermore, it is demonstrated that the formation of the prevailing mode of the extratropical atmospheric general circulation is closely associated with the feature that the PPE has both a zonal symmetry on global scale and zonal asymmetry on local scale. Moreover, there is a significant correlation between the first two orders of moments of the PPE and the southern/northern annular mode indices in the winter, but such a relationship is apparently weakened in the summer and exists in the southern hemisphere only.

Key words Perturbation potential energy, Atmospheric general circulation anomaly, Kinetic energy, Annular mode, SVD

1 INTRODUCTION

Atmospheric energetics is of particular importance in atmospheric dynamics. In terms of the classical atmospheric energetics, atmospheric total potential energy (TPE) can be decomposed into two parts: available part and unavailable part, where the former may be released and transformed into kinetic energy (KE) and the latter may not[1−3]. This is referred to as the issue of energy availability (EA). For this issue, the conception of atmospheric available potential energy (APE) is usually used to demonstrate the TPE-KE transform, energy cycle and maintenance of atmospheric general circulation, which has also been applied to studies on oceanic energetics[4−14]. However, the previous studies only concentrated on the global mean APE which can solely reflect the whole EA of atmospheric system. Therefore, this global-mean-based APE framework is not suitable for the study of local energetics.

Actually, the features of weather/climate systems and their anomalous occurrences usually have apparent locality[15−17]. There is an intimate relationship between local atmospheric motion variations and local EA. The budget, distribution and transformation of atmospheric energetics have significant local characteristics. Further, generation and development of weather/climate phenomena are so evidently associated with local energy source/sink which exists inside atmospheric system that anomalous variations of local energetics will definitely have a significant influence on local atmospheric general circulation. Therefore, it is fairly important to examine the efficiency and mechanism of regional energy transformation for understanding local atmospheric circulation variations. This is just the issue of local energy availability (LEA). In our previous studies[17−18],

E-mail: gaol@cma.gov.cn

the conception of local perturbation potential energy (PPE), which is suitable to addressing the LEA, has been proposed in order to handle the relevant questions of the transformation between the local TPE and KE. To better understand the basic conception of PPE, the spatio-temporal characteristics and interannual variability were examined in the existed studies[17−20].

In this paper, based on the prior studies, a statistical tool of singular value decomposition (SVD) will be used to examine the coupled relationships between the PPE and different atmospheric motion and state variables, and aim to reveal the primary coupled correlation patterns as well as the mechanism of their impacts on atmospheric circulation anomalies. The focus will be on analyzing the coupled correlation patterns and their interannual variability between the PPE and the atmospheric KE at higher, middle and lower pressure levels, and on examining the relationship between the PPE and the sea level pressure (SLP) as representing atmospheric mass distribution, and on discussing the associated mechanism between the PPE and the KE and SLP.

2 DATA AND METHOD

The data used here is from the National Center for Environment Prediction/ National Center for Atmospheric Research (NCEP/NCAR) reanalysis dataset[21]. The period that this study covers is the wintertime (Nov-Mar) from 1948 through 2004 and the resolution of horizontal grid point is taken as $5^\circ \times 5^\circ$. The analyzed domain is over the northern hemispheric extratropics (north of 20°N). The variables addressed are the PPE integrated at all vertical levels and atmospheric KE at 200 hPa, 500 hPa and 850 hPa. Other data include the sea level pressure of the NCEP/NCAR reanalysis and the extended reconstructed sea surface temperature (SST) of the National Climate Data Center. The SVD method is used to obtain the coupled correlation patterns between the PPE and the KE and SLP, for details of the method refer to the Appendix.

3 COUPLED RELATIONSHIPS BETWEEN PPE AND KE

In the previous studies[17−20], we have analyzed the spatiotemporal characteristics of different components of the PPE and found their apparent associations with the KE. Therefore, to examine the coupled relationships between the PPE and KE, we first do the SVD analysis by taking the winter 500-hPa KE at the northern hemispheric extratropics as the left field and taking the vertically-integrated PPE as the right field.

Table 1 presents information of the first five SVDs of 500-hPa kinetic energy and PPE. It is seen that there is a clear "gap" of the percentage of explained covariance square summation (CSS) between the first two patterns and the third and fourth modes. The first three SVD modes explain accumulatively greater-than-60% total CSS between the left and right fields, which can represent the main features of the coupled modes of the two fields. The first SVD mode explains 30.3% of the total CSS, 8.4% of the 500-hPa KE variance and 12.83% of the PPE variance, respectively. This indicates that the principal coupled mode takes up a large variance percentage (VP) in the PPE field but a relatively small VP in the KE, which also reflects that the KE has a more complicated feature than the PPE. On the other hand, for most of the coupled modes, their correlations between the extension coefficients (ECs) of the left and right fields can reach 0.8∼0.9, significant statistically at the 99.9% confidence level.

Table 1 Information of the first 5 SVDs of 500 hPa kinetic energy (left) and PPE (right)

No.	Singular values	Explained CSS/(%)	Accumulatively explained CSS/(%)	Correlations between ECs	Explained VP of the left/(%)	Explained VP of the right/(%)
1	92.1	30.30	30.30	0.908	8.40	12.83
2	67.6	16.32	46.61	0.898	6.78	8.77
3	62.6	14.00	60.61	0.849	6.41	9.33
4	52.6	9.90	70.51	0.799	4.99	10.63
5	41.2	6.07	76.58	0.858	5.78	4.80

Note that the SVD modes prefer to reflect the relationships between two fields as much as possible rather than the either individual variability. As a result, although the first 10 modes have the singular values which decrease linearly (all greater than 0), their contributions to explaining variance of either field do not certainly decrease in the same sequence. In contrast, the first coupled SVD mode can explain the biggest percentages in both the variances and the covariance. Therefore, the emphasis in the following will be put on the spatio-temporal feature of the first mode.

Figure 1 shows the homogeneous and heterogeneous correlation maps as well as the extension coefficients for the first mode of the left and right fields. This mode can explain 30.3% of the total covariance, reflecting its predominance in the coupled relationship. Indeed, the contributions that the first mode makes to the variance of either the left or the right field is relatively smaller than that to their covariance. Also, such a coupled mode

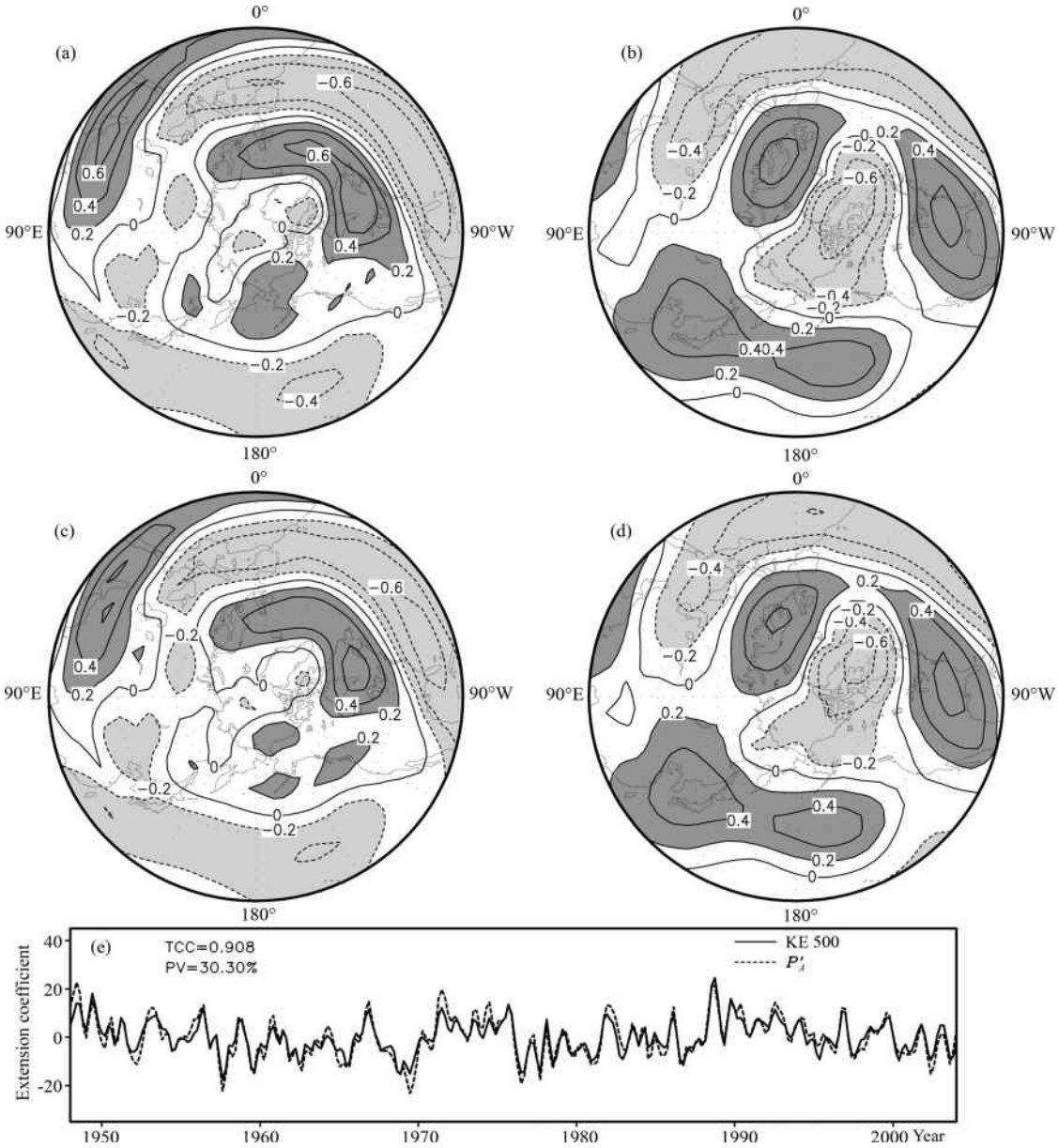

Fig. 1 The first SVD of winter 500 hPa kinetic energy (left) and PPE (right)

Panels (a) and (b) are the left and right homogeneous correlation maps, (c) and (d) the left and right heterogeneous correlation maps, (e) the extension coefficient series of the left and right fields with a 3-point running mean. The dark (or light) shadings denote the significant positive (or negative) correlation areas at the 95% confidence level. The outmost latitude is at 20°N and longitudinal interval is 20°. Contour interval is 0.2. TCC: temporal correlation coefficient; PV: percentage of variance.

may play slightly different role in either of the fields. It is found that the left heterogeneous correlation pattern is quite similar to the first empirical orthogonal function (EOF) pattern of the standardized KE deviation, and the right heterogeneous correlation pattern is quite similar to the first EOF of PPE as well. In the left homogeneous correlation pattern, the significant features are the positive correlations which distribute over the North America–North Atlantic region and the North Africa–South Asian region, and the negative correlations which are annularly located in the subtropics. In the right homogeneous correlation pattern, the significant positive correlations are mainly resided in the south of South America, West Europe and North Pacific regions, and the significant negative correlations are located in the north of North America and the subtropical Atlantic - North African regions. Except the polar regions, the high latitudes north of 50°N are covered by positive correlations and the mid-latitude areas are covered by negative correlations. It is also seen in Fig. 1 that the heterogeneous and homogeneous correlation patterns for the left and right fields are almost same, which indicates clearly that the first SVD mode is not only dominant in the covariance of the two fields, but also in the individual variance.

In Fig. 1e, it is seen that the temporal extension coefficients of the left and right fields are highly correlated (0.908), indicating a perfect coupled relationship between the PPE and KE fields. Consequently, the corresponding temporal coefficients have overall the same signs between the left and right fields. This suggests that the variation of the KE is largely coherent with the non-zero variations of the PPE.

Next, we further examine the characteristics of the high-level and low-level KE and their coupled relationships with the PPE. Thus, the SVD analysis is operated by taking the vertically-integrated PPE as the right field and the extratropical 200-hPa or 850-hPa KE north of 20°N as the left field, respectively.

To quantify the relationship between the PPE and 200-hPa KE, Table 2 presents the information for the first five SVDs. This information is basically analogical to that of 500 hPa. That is, the first SVD mode explains 32% of the TCS between the two fields, and 11.04% and 13.49% of the variances of the KE and PPE, respectively. Compared to 8.4% and 12.83% of 500-hPa level, the coupled mode becomes more important in the individual variation with height increasing. Moreover, the TCS explained by the first three SVD modes reaches 63%, which indicates these modes are able to represent the main features of the coupled variations between the two fields. Most of the correlations between the extension coefficients of the left and right fields reached 0.8∼0.9, which are significant at the 99.9% confidence level.

Table 2 Information of the first 5 SVDs of 200 hPa kinetic energy (left) and PPE (right)

No.	Singular values	Explained CSS/(%)	Accumulatively explained CSS/(%)	Correlations between ECs	Explained VP of the left/(%)	Explained VP of the right/(%)
1	107.8	31.57	31.57	0.904	11.04	13.49
2	79.4	17.13	48.70	0.882	8.86	9.93
3	72.1	14.10	62.79	0.918	7.64	8.38
4	57.9	9.09	71.89	0.835	5.26	10.56
5	44.4	5.36	77.24	0.897	5.30	5.32

The correlation coefficients corresponding to the first SVD mode are shown in Fig. 2. It is clear that the spatial patterns of singular eigenvectors between the 200-hPa KE and the PPE appear to be almost completely opposite to those at 500 hPa, and the evolutions of time coefficient series are almost opposite as well. It is actually easy to understand that based on the previous studies[14−15], the PPE has an opposite sign at 200 hPa, compared to the middle-lower levels, which yields the opposite distributions in the SVD. Indeed, this situation has no impact on the eventual conclusions in this study because the patterns at the two levels will become consistent as long as both the singular eigenvectors and time coefficients are factored by –1. For the homogeneous and heterogeneous maps, the spatial patterns at 200 hPa are fairly consistent with those at 500 hPa, where the former appears to be more regular, smoother and more zonally symmetric than the latter. Still, the two extension coefficient series are highly correlated (0.904).

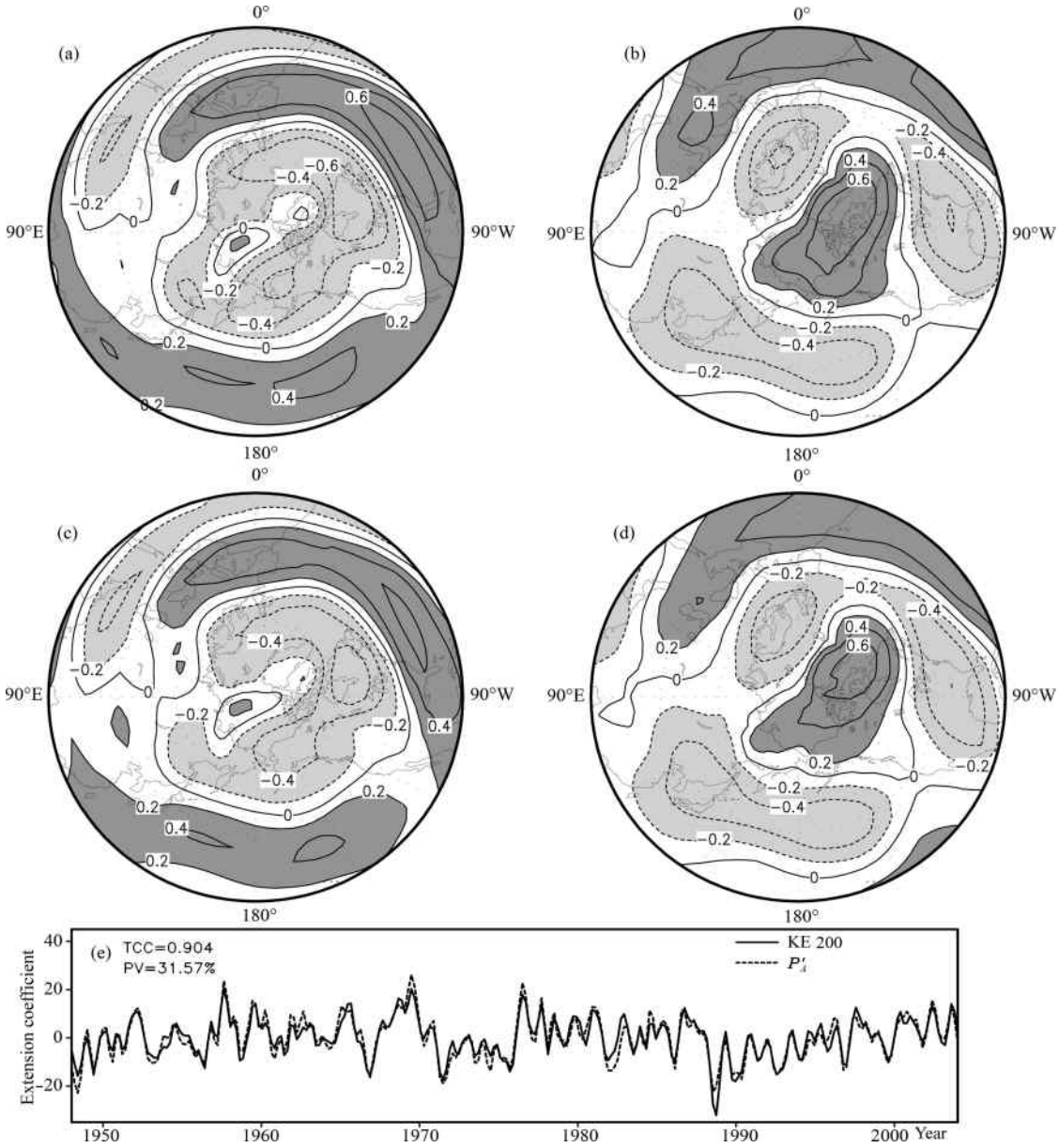

Fig. 2 The same as Fig. 1, but for the 200 hPa kinetic energy as the left field

In Table 3, we further give the information for the first five SVDs between the PPE and 850-hPa KE, which looks basically similar to that at 500 hPa. The first SVD mode explains 34% of the TCS between the two fields, and 7.09% and 12.87% of the variances of the KE and PPE, respectively. The TCS explained by the first three SVD modes reaches 60%, indicating that the modes can represent the major features of the two coupled fields. Indeed, these "gaps" in the explained variance percentages can be taken as the natural scale truncation in the diagnostic analysis, such as those between the second and third mode as well as those between the fourth and fifth modes. Also, it is seen that the correlations between the extension coefficients of the left and right fields mostly exceed 0.8∼0.9, significant at the 99.9% confidence level.

Figure 3 shows the correlation coefficients corresponding to the first mode. It is clearly seen that the singular eigenvector patterns between the 200-hPa KE and the PPE are fairly similar to those between the 500-hPa KE and the PPE. In particular, the homogeneous and heterogeneous maps for the right field, the two spatial patterns at 850 hPa are not only consistent with those at 500 hPa, but also similar to each other. In contrast, the two correlation maps for the left field are also similar to each other, which are slightly different

from those of 500 hPa over the North Pacific. This reflects that the coupled modes between the two variables are basically consistent in the middle-lower-level atmosphere. The two time series of extension coefficient appear to be highly correlated (0.88) with each other, which is slightly lower than that of 500 hPa, however, the evolutions of the two time series are almost same.

Table 3 Information of the first 5 SVDs of 850 hPa kinetic energy (left) and PPE (right)

No.	Singular values	Explained CSS/(%)	Accumulatively explained CSS/(%)	Correlations between ECs	Explained VP of the left/(%)	Explained VP of the right/(%)
1	81.2	33.55	33.55	0.877	7.09	12.87
2	54.3	15.03	48.57	0.858	4.68	9.46
3	46.9	11.21	59.78	0.822	4.28	8.55
4	45.1	10.34	70.12	0.760	4.28	10.79
5	33.5	5.72	75.84	0.817	4.15	4.91

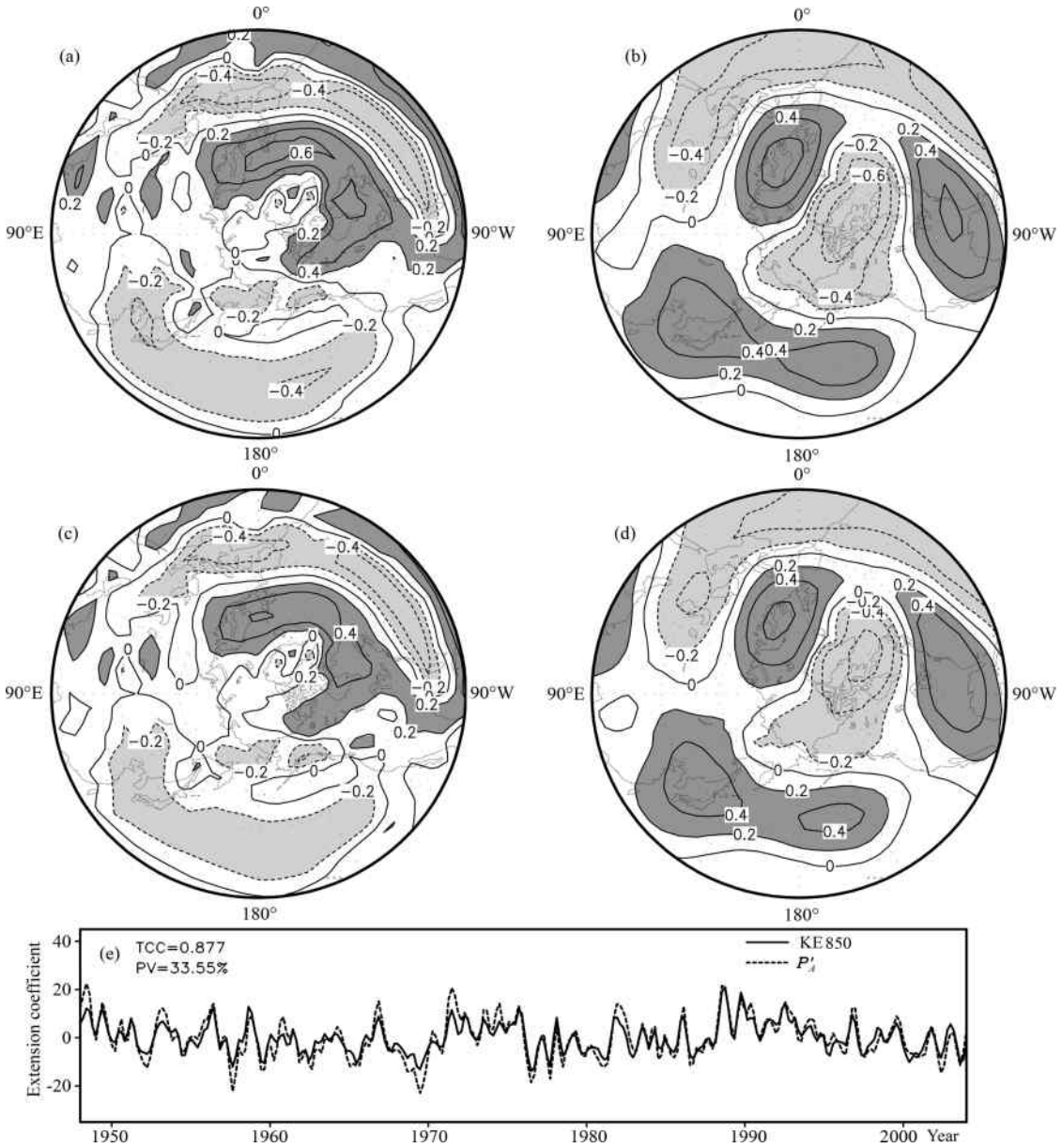

Fig. 3 The same as Fig. 1, but for the 850 hPa kinetic energy as the left field

4 COUPLED RELATIONSHIPS BETWEEN PPE AND SLP

As we know, anomalous variations of atmospheric motion can yield a change of atmospheric mass distribution, and thus an anomalous variation of SLP. Therefore, to understand the anomalous association between the PPE and atmospheric mass, we here will examine the relationships between them through the SVD analysis by taking the SLP north of 20°N in the winter northern hemisphere as the left field and the vertically-integrated PPE as the right field. This analysis will help us understand the relationships between the atmospheric energy availability and the dynamical features of atmospheric general circulation.

We give the information for the first five SVDs between the PPE and SLP in the mid-high latitudes in Table 4. The first SVD mode explains 44.69% of the TCS between the two fields, and 21.93% and 13.08% of the variances of the SLP and PPE, respectively. That is, the first coupled correlation mode is dominant and explains most of the variance in the SLP field. This situation does not appear in the analysis results regarding the atmospheric KE, which reflects that given a known principal spatial pattern of the PPE, its corresponding time coefficients can represent the typical spatial distribution of the SLP field. The TCS explained by the first three SVD modes reaches 72.42%, which indicates that the modes can represent the main features of the two coupled fields. For most of the coupled modes, the correlations between the corresponding extension coefficients between the left and right fields exceed 0.8, significant at the 99.9% confidence level.

Table 4 Information of the first 5 SVDs of mid-high-latitude SLP (left) and PPE (right)

No.	Singular values	Explained CSS/(%)	Accumulatively explained CSS/(%)	Correlations between ECs	Explained VP of the left/(%)	Explained VP of the right/(%)
1	131.90	44.69	44.69	0.816	21.93	13.08
2	75.09	14.49	59.18	0.832	9.29	9.73
3	71.81	13.25	72.42	0.861	8.80	9.09
4	55.84	8.01	80.43	0.841	5.97	8.49
5	41.94	4.52	84.95	0.867	5.39	5.13

Further, Fig. 4 shows the homogeneous correlation, heterogeneous correlation, and time extension coefficient corresponding to the first SVD mode. It is found that the left heterogeneous correlation pattern is quite similar to the first EOF pattern of the normalized SLP (not shown), whereas the right heterogeneous correlation pattern is similar to the first eigenvector pattern of the first-order moment of the PPE[17]. In Fig. 4, on one hand, the homogeneous and heterogeneous correlation patterns are fairly similar, i.e., significant negative correlations over the polar region and significant positive correlations over subtropics, especially, over the North Pacific and North Atlantic. On the other hand, the two correlation patterns for the right field are almost same and it is more important that they both are also consistent with those corresponding to the coupled modes of the PPE and atmospheric KE. These clearly indicate that the first mode of the PPE is likewise the principal mode of the coupled variations between the PPE and atmospheric general circulation anomalies, and the primary modes of the corresponding atmospheric KE and mass fields are also the dominant modes of their own variability. Therefore, there possibly exists a physical mechanism that contributes to generating the co-variability between the PPE and atmospheric general circulation anomalies.

Indeed, in the right heterogeneous correlation pattern, there is a slightly different feature from other similar correlation patterns; i.e., the negative correlations tend to be separated into two independent centers, located in the North Pacific and in the North Atlantic, respectively, which is not present on the homogeneous correlation maps. In this case, noting the positive correlations over the North Pacific and North Atlantic in the correlation patterns of the left field, and considering the dominant role of the PPE in generating local or regional circulation, we can infer that by taking 60°E–120°W as a boundary in the PPE patterns, the positive/negative centers of the PPE over the Atlantic supply the available energy for the Atlantic section of the left field, whereas the positive/negative centers of the PPE over the Pacific provide the available energy for the Pacific section of the

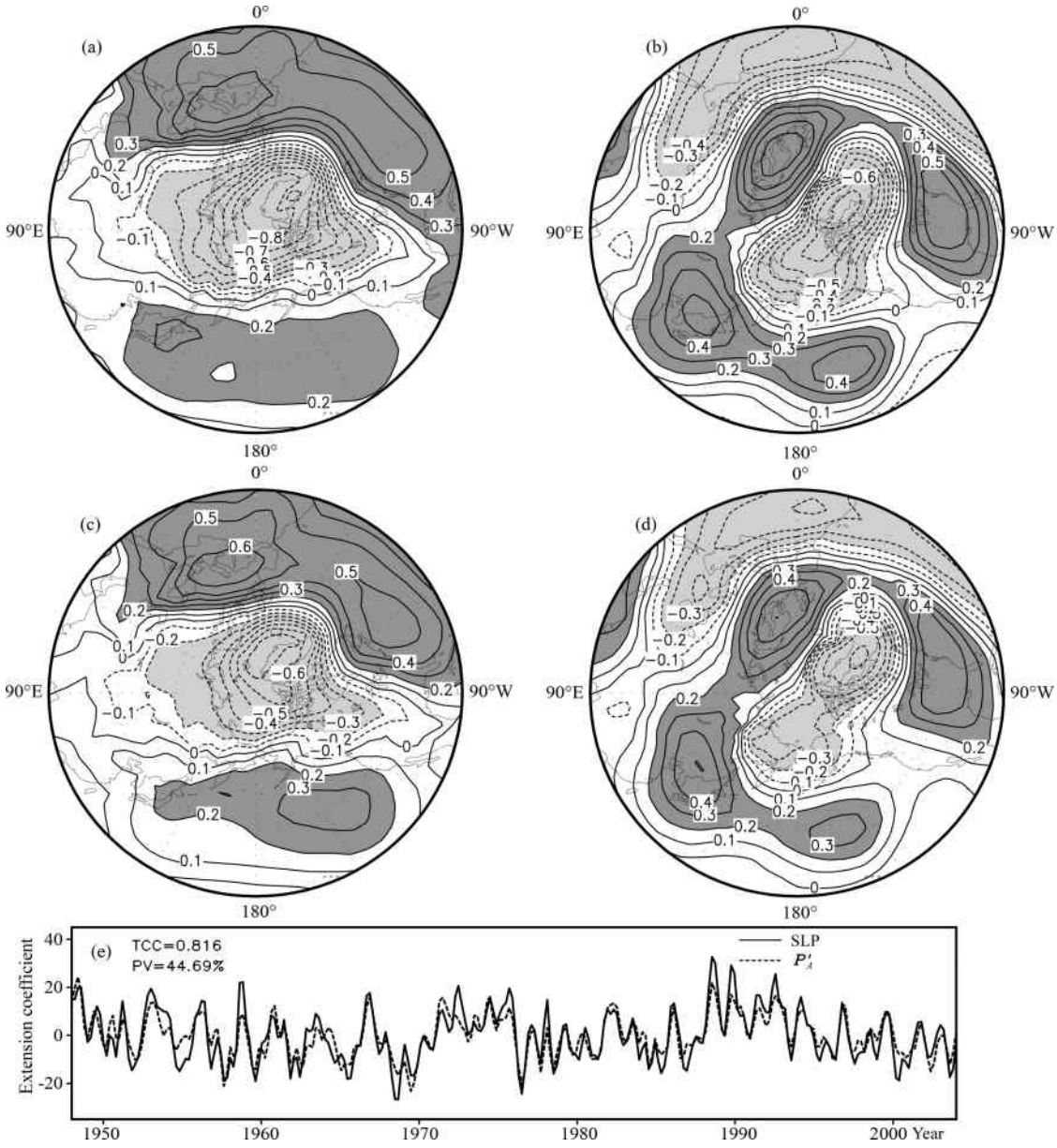

Fig. 4 The same as Fig. 1, but for the SLP as the left field, where contour interval is 0.1

left field. This phenomenon still needs further verification. Moreover, the correlation coefficient between time coefficient series of the left and right fields is approximately 0.82, which is slightly lower than those in the fore-mentioned correlation coefficients.

5 INTEGRATED ANALYSIS AND DISCUSSION ON THE PPE-KE RELATIONSHIP

Based on the anterior correlation analyses between the PPE and the high, middle, and low-level atmospheric KE, it is clearly seen that the primary coupled correlation patterns all have an out-of-phase contrast between mid-high latitudes and subtropics with a global annular distribution, especially on the 200-hPa map. In contrast, the KE has a more regular annular or zonally symmetric structure, whereas the PPE has an increased zonal asymmetry and tends to include three action centers at the southern South America, western Europe and North Pacific regions. By further contrasting with the SVD results of the PPE and SLP, we find that the principal pattern of atmospheric mass field also has an out-of-phase structure between mid-high latitudes and

subtropics, which is actually consistent with the features of the famous Arctic or Antarctic oscillations[22−26]. That is, there is a global-scale zonal annular action belt and two significant action centers which are located over the North Pacific and North Atlantic, respectively. The implication of the analysis is that from a point of view of atmospheric thermodynamics, the generation of the principal mode of extratropical atmospheric general circulation is intimately related to the fact that the principal PPE pattern has both the global-scale zonally symmetric structure and the local-scale zonally asymmetric structure. This may provide a new insight into the polar oscillation phenomenon through focusing on the energetic availability. On one hand, since the PPE used here is integrated vertically, it has a consistent coupled mode features with either the atmospheric KE at different levels or the SLP, with the apparent asymmetric and localized patterns. This implies that the energy availability, which is influenced directly by thermal forcing, may be generated as a result of both the equator-pole temperature difference and the land-sea contrast. The former tends to contribute a zonally symmetric annular structure and the latter appends a zonal asymmetries. It is conceivable that under the condition of the pure driving due to the equator-pole difference, the fist coupled mode pattern should have a feature with a completely zonally symmetric annular distribution. However, due to the irregular thermal heating induced by the land-sea contrast, this coupled SVD-mode pattern become to have both the regular annular structure and the zonal asymmetries to some degree.

On the other hand, as we know, many previous studies have revealed that the PPE is a physical source of the atmospheric KE. Based on the above results, it can be easily found out that the APE in a global sense is actually an integration of the PPE that is much different locally. Because the PPE is still regarded as a whole in this study, the first-order moment of the PPE has a zero global net contribution while the second-order moment of the PPE makes a primary contribution to the global APE even though the surface PPE may be contributive as well. Therefore, considering the significant local characteristics in the major coupled SVD patterns, the first-order moment of the PPE definitely makes a crucial contribution to the local and global atmospheric KE, and in this case its net contribution to the global mean is evidently nonzero. Indeed, the second-order moment of the PPE need to be considered as well through an additional SVD analysis of the individual components of the PPE and the KE. Moreover, under the action of the same dominant PPE mode, the atmospheric KE is manifested by the slightly different correlation modalities at the different vertical levels; i.e., with height going up, the primary coupled patterns associated with the KE become more zonally symmetric.

In addition, it is worthy of note that the significant positive/negative anomalies (where the heterogeneous correlation patterns are completely consistent with the singular eigenvector patterns of the SVD, only different in their magnitude) have zero lines which is likely in consistence with the trough/ridge lines of the positive/negative anomalies of the KE at the different levels. Thereby, if we add the zero lines of the PPE patterns on the homogeneous and heterogeneous correlation patterns of the KE (refer to Figs. 1–3), it can be clearly seen that the zero lines of the primary patterns of the PPE are basically consistent with the centers of the anomaly extrema of the KE patterns. The reason of concerning the PPE zero lines is that the positive (negative) PPE anomalies are likely corresponding to the external heating (cooling) sources, which lead to the air temperature increasing (decreasing) and thus the local PPE greater (less) than the global mean. Thus, the PPE zero lines are located between the relative heating and cooling regions, where the maximum wind speed appears in terms of the thermal wind rule. Indeed, another worth point of view is that in terms of the transform relationship between the PPE and the atmospheric KE, the relative transform between them will be the most complete when the PPE anomaly becomes zero, the time that the KE anomaly is maximum.

6 CORRELATION OF PPE WITH MID-HIGH-LATITUDE ANNULAR MODE INDICES

As we have known, the northern-hemispheric annular mode index (NAMI) and southern-hemispheric annular mode index (SAMI) are usually used to represent the variation features of the mid-high-latitude atmospheric general circulation. That is, the high (low) index values indicate the enhanced (reduced) subtropical high, deepened (shallow) subpolar low, strengthened (weakened) mid-latitude westerly and zonally (meridionally)

distributed circulation regime. Based on the previous analyses, it will be implicative to examine the characteristics of the PPE that are associated with these global-scale annular modes. Since the summation of the first two order moments of the PPE have been used in the above analyses, we here will analyze separately the correlations between the first-order and second-order moments of the PPE and the two annular mode indices by taking January and July data as representing typical months of the boreal wintertime and summertime, respectively, which can also provide a reference to the next detailed SVD field analysis.

Figures 5 and 6 show the correlations between the boreal winter NAMI and SAMI and P'_{A1} and P'_{A2}, respectively. It is clear that the correlation patterns associated with NAMI basically take on zonally symmetric annular distributions, and interestingly, the correlations for P'_{A1} and P'_{A2} are out of phase, which can be more clearly seen in the zonally averaged correlation curves. There are similar correlation patterns for SAMI, where the differences are only that the annular patterns are not as excellent as those for NAMI due to the boreal summertime. Also, the out-of-phase relationship between the two moments is clear, as shown in Fig. 6. Overall, for the northern-hemispheric extratropics, the zonal circulation regime at the middle latitudes is characterized by higher subtropical P'_{A1} and lower P'_{A2}, as well as lower subpolar P'_{A1} and higher P'_{A2}, which is completely caused by the anomalous variations of the extratropical perturbation temperature T'.

Further, Figs. 7 and 8 show correlations between the boreal summer NAMI and SAMI and P'_{A1} and P'_{A2}, respectively. It is seen that different from Fig. 5, in the northern-hemispheric mid-high latitudes, there are no robust correlation distributions, but a few isolated centers, which are similar between the two moments. The

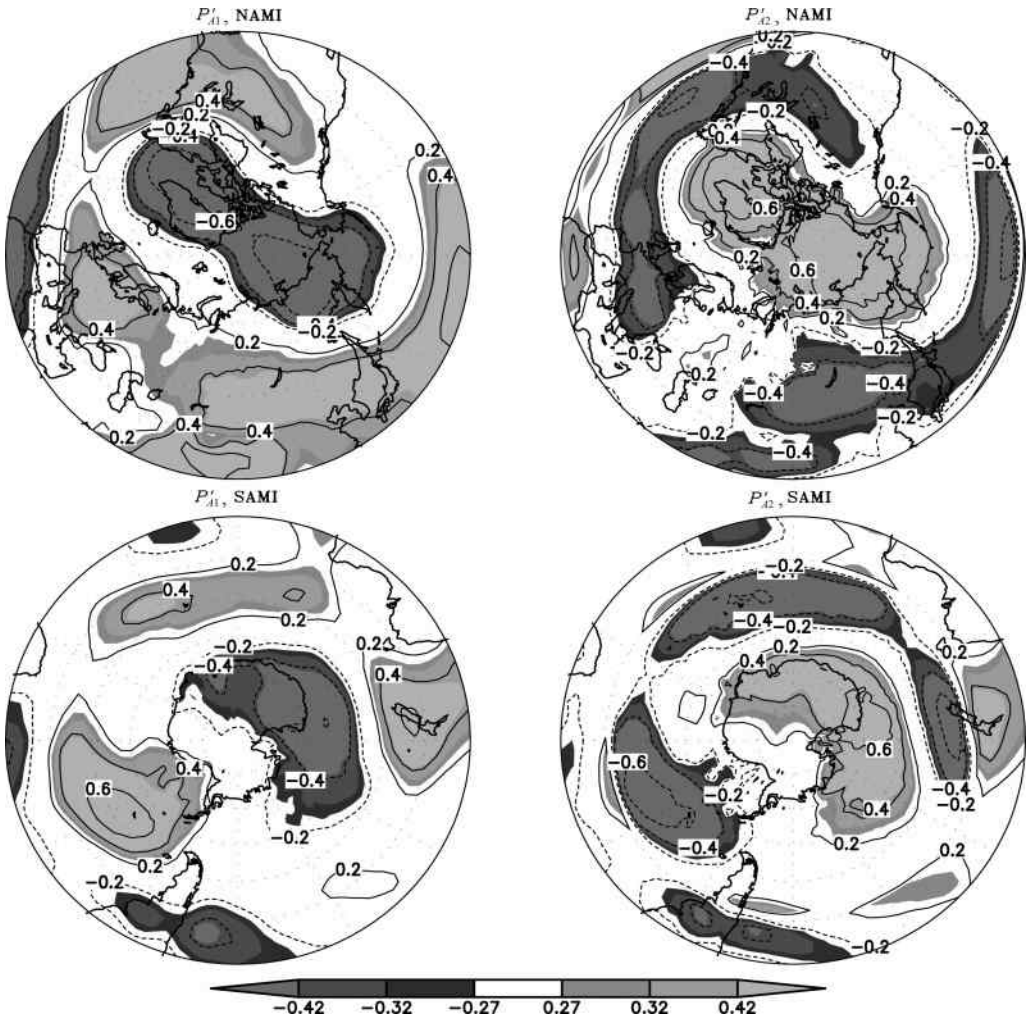

Fig. 5 Correlations between January NAMI/SAMI and P'_{A1}/P'_{A2}

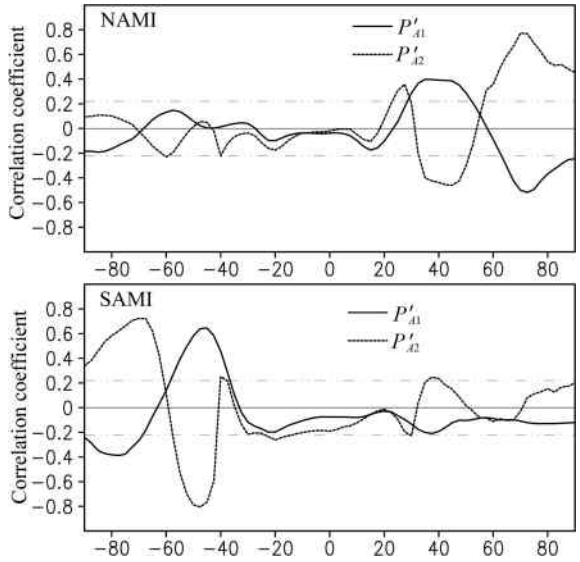

Fig. 6 Zonal-mean correlations between January NAMI/SAMI and P'_{A1}/P'_{A2}

situations in the southern hemisphere become much better than those in the northern. Not only there are the significant correlations appearing in the Antarctic continent, but also the out-of-phase correlations in the surrounding areas, which is only slightly weaker than the boreal winter. Indeed, this may be worthy of note because it is generally believed that the cold-season circulation is far more regular than the warm-season circulation whereas the results here show an opposite situation. Moreover, it can be found that whether NAMI or SAMI has better correlations with P'_{A1} than P'_{A2}, and particularly, NAMI seems to have much higher correlations with the southern-hemispheric P'_{A1} than the northern hemispheric, for which the reason is still unclear and needs further investigations. In the boreal wintertime, the significant correlation pattern for NAMI is annularly distributed on the whole, and the

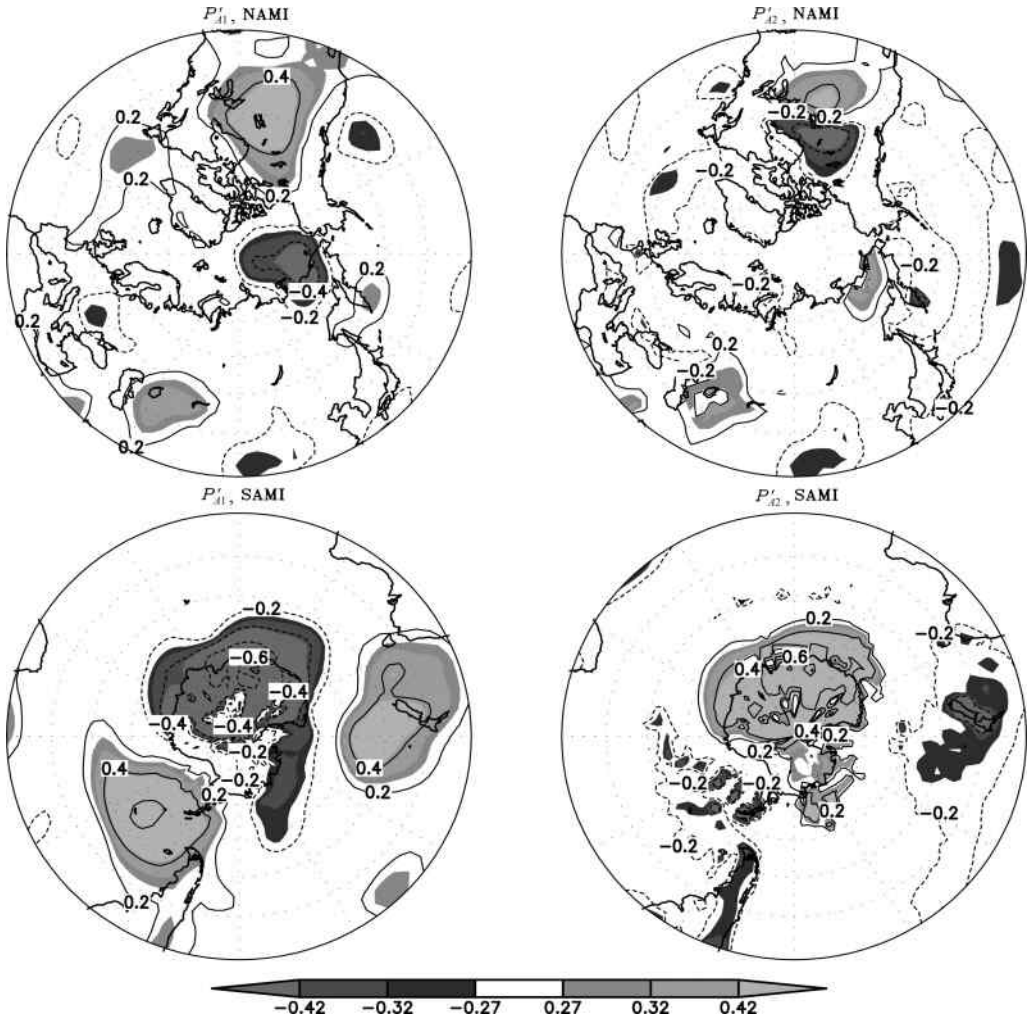

Fig. 7 The same as Fig. 5, but for July

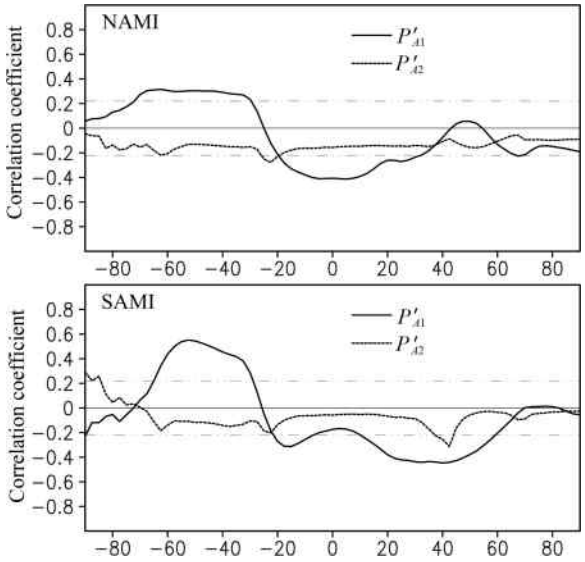

Fig. 8 The same as Fig. 6, but for July

correlation distributions are opposite in the tropics between P'_{A1} and P'_{A2}. The similar situations are for SAMI, which can be also clearly seen in Fig. 6.

7 SUMMARY AND DISCUSSION

This study focuses on the relationships between the PPE and the atmospheric general circulation anomalies. The SVD analysis method has been applied to the examinations of the coupled correlation modes and interannual variability between the PPE and the atmospheric KE, and of the relationship between the PPE and the SLP. Based on these analyses, the associated mechanism has been preliminarily examined for the relationships between the PPE and the atmospheric KE and SLP.

The results show that the first mode of the PPE variability is the principal mode of the co-variability between the PPE and the atmospheric general circulation fields, and the corresponding primary coupled modes between the PPE and the atmospheric KE and SLP are also the dominant modes in their own variability. This indicates there may be a mechanism which restricts the co-variability of the PPE and the general circulation anomalies. Furthermore, the formation of the primary patterns of the extratropical atmospheric circulation is intimately linked with the fact that the PPE has both the global-scale zonally symmetric structure and the local-scale zonal asymmetries. Moreover, the excellent correlations exist between the boreal-winter NAMI and SAMI and the first two order moments of the PPE, which become reduced in the boreal summertime and are only located in the southern hemisphere.

Indeed, most of the analyses in this study have focused on the whole PPE instead of its individual components except the examinations of the correlations between the mid-high-latitude circulation indices and the PPE, in order to make the story simple and the points clear. In the next, to obtain the more detailed physical pictures of the coupled variations and mechanisms, we are going to conduct the SVD analysis for the relationship between the separated PPE components and the atmospheric circulation anomalies. In addition, we may further concern a new conception of the moist PPE because many moist physical processes usually play crucial roles in generating the climate variability[27−28] even though it was considered in previous studies[29].

APPENDIX: SINGULAR VALUE DECOMPOSITION

Singular value decomposition (SVD) has been broadly applied in meteorological research. The SVD is one of the best method separating coupled patterns from two fields, which is quite concise, easily understood, and independent on any parameter without systematic errors. Principle and application of the SVD analysis can be found in many literatures and textbooks. To make the current analysis easy, the method will be briefly introduced in the following.

To two arbitrary scalar fields, $S_i(t)$ denotes observation of one variable at the i spatial point, and $Z_j(t)$ denotes observation of another variable at the j spatial point, which are usually termed the left and right fields, respectively. Here, $i = 1, 2, \cdots, N_{\rm S}, j = 1, 2, \cdots, N_{\rm Z}$ and $t = 1, 2, \cdots, T$. In general, $N_{\rm S}$ may not be equal to $N_{\rm Z}$.

Set the covariance matrix of the two fields as $\boldsymbol{C}_{\rm SZ}$, then $\boldsymbol{C}_{\rm SZ} = S_i(t)Z_j^{\rm T}(t)$, which is a matrix of size $N_{\rm S} \times N_{\rm Z}$. If $S_i(t)$ and $Z_j(t)$ are standardized data, $\boldsymbol{C}_{\rm SZ}$ will be a correlation matrix. The SVD of $\boldsymbol{C}_{\rm SZ}$ is as

follows

$$\boldsymbol{C}_{\mathrm{SZ}} = \sum_{k=1}^{R} \sigma_k p_k q_k^{\mathrm{T}},\ R \leq \min(N_{\mathrm{S}}, N_{\mathrm{Z}}), \tag{A1}$$

where, p_k is one of the R orthogonal left singular vectors of $\boldsymbol{C}_{\mathrm{SZ}}$, q_k is one of the R orthogonal right singular vectors of $\boldsymbol{C}_{\mathrm{SZ}}$, which represent the typical distributions of the left and right fields, respectively. σ_k is the singular value of $\boldsymbol{C}_{\mathrm{SZ}}$, where $\sigma_1 \geq \sigma_2 \geq \cdots \geq \sigma_k \geq \cdots \geq \sigma_R > 0$.

In terms of the orthogonality between the singular vectors, the time coefficients (i.e., extension coefficients or principal components) can be expressed as follows

$$a_k(t) = P_k^{\mathrm{T}} S(t) = \sum_{i=1}^{N_{\mathrm{S}}} p_{ki} S_i(t), \tag{A2}$$

$$b_k(t) = Q_k^{\mathrm{T}} Z(t) = \sum_{i=1}^{N_{\mathrm{Z}}} q_{kj} Z_j(t), \tag{A3}$$

$a_k(t)$ and $b_k(t)$ stand for the time coefficients corresponding to the k pair of singular vectors of $S_i(t)$ and $Z_j(t)$, whose covariance just is the singular value σ_k. Therefore, the correlation between $a_k(t)$ and $b_k(t)$ is

$$r_k = \frac{\sigma_k}{\frac{1}{T}\sqrt{\sum_{t=1}^{T} a_k^2(t) \sum_{t=1}^{T} b_k^2(t)}}. \tag{A4}$$

The percentage of the squared covariance explained by the k pair of spatial canonical distribution is

$$\mathrm{SCF}_k = \frac{\sigma_k^2}{\sum_{k=1}^{R} \sigma_k^2} \times 100\%. \tag{A5}$$

If taking the first $N(N \leq R)$ pairs of spatial canonical distributions, the explained accumulated covariance square has a percentage as

$$\mathrm{SCF}_k = \frac{\sum_{k=1}^{N} \sigma_k^2}{\sum_{k=1}^{R} \sigma_k^2} \times 100\%. \tag{A6}$$

After obtaining $a_k(t)$ and $b_k(t)$, the coupled spatial canonical distribution patterns can be generally obtained through analyzing the left and right singular vectors directly. However, the more ordinary procedure is to analyze two kinds of correlation maps, homogeneous and heterogeneous correlations. If set $r[f(t), g(t)]$ for denoting the correlation between the two series of $f(t)$ and $g(t)$, the k left (right) homogenous map (which are expressed by $\boldsymbol{r}[S_i(t), a_k(t)]$ and $\boldsymbol{r}[Z_j(t), b_k(t)]$, respectively) can be obtained from the correlation between the left (right) and the k left (right) time coefficients. In the similar way, the k left heterogeneous map can be obtained through $\boldsymbol{r}[S_i(t), b_k(t)]$ and the k right heterogeneous correlation $\boldsymbol{r}[Z_j(t), a_k(t)]$.

For the homogeneous correlation, the percentage of the k pair of time coefficients explaining the variances

for the left and right fields can be estimated as

$$\mathrm{VFL}_k = \frac{\sum_{t=1}^{T} a_k^2(t)}{\sum_{k=1}^{R}\sum_{t=1}^{T} a_k^2(t)} \times 100\% = \frac{\frac{1}{T}\sum_{t=1}^{T} a_k^2(t)}{N_\mathrm{S}} \times 100\%, \tag{A7}$$

$$\mathrm{VFR}_k = \frac{\sum_{t=1}^{T} b_k^2(t)}{\sum_{k=1}^{R}\sum_{t=1}^{T} b_k^2(t)} \times 100\% = \frac{\frac{1}{T}\sum_{t=1}^{T} b_k^2(t)}{N_\mathrm{Z}} \times 100\%. \tag{A8}$$

If take N pairs of time coefficients, the percentage regarding the accumulated variance will be

$$\mathrm{VFL}_N = \frac{\sum_{k=1}^{N}\sum_{t=1}^{T} a_k^2(t)}{\sum_{k=1}^{R}\sum_{t=1}^{T} a_k^2(t)} \times 100\% = \frac{\sum_{k=1}^{N}\frac{1}{T}\sum_{t=1}^{T} a_k^2(t)}{N_\mathrm{S}} \times 100\%, \tag{A9}$$

$$\mathrm{VFR}_N = \frac{\sum_{k=1}^{N}\sum_{t=1}^{T} b_k^2(t)}{\sum_{k=1}^{R}\sum_{t=1}^{T} b_k^2(t)} \times 100\% = \frac{\sum_{k=1}^{N}\frac{1}{T}\sum_{t=1}^{T} b_k^2(t)}{N_\mathrm{Z}} \times 100\%. \tag{A10}$$

For the heterogeneous correlation, the percentage of the k pair of time coefficients explaining the variances for the left and right fields can be estimated as

$$\mathrm{VFL}_k = \frac{\sum_{i=1}^{N_\mathrm{S}} r^2[b_k(t), S_i(t)]}{N_\mathrm{S}} \times 100\%, \tag{A11}$$

$$\mathrm{VFR}_k = \frac{\sum_{j=1}^{N_\mathrm{Z}} r^2[a_k(t), Z_j(t)]}{N_\mathrm{Z}} \times 100\%. \tag{A12}$$

The percentage regarding the accumulated variance explained by the N pairs of time coefficients will be

$$\mathrm{VFL}_N = \frac{\sum_{k=1}^{N}\sum_{i=1}^{N_\mathrm{S}} r^2[b_k(t), S_i(t)]}{N_\mathrm{S}} \times 100\%, \tag{A13}$$

$$\mathrm{VFR}_N = \frac{\sum_{k=1}^{N}\sum_{j=1}^{N_\mathrm{Z}} r^2[a_k(t), Z_j(t)]}{N_\mathrm{Z}} \times 100\%. \tag{A14}$$

It is worthy of note that to obtain the two kinds of correlation maps, the left and right fields may not certainly be fixed in the spatial domain where the SVD analysis was done, but may be enlarged somewhat. Generally speaking, a homogeneous correlation pattern is not proportional to a singular vector, whereas a heterogeneous correlation pattern is positively proportional to a singular vector. Indeed, a homogeneous pattern can reflect well the polarity and amplitude of the spatial patterns that correspond to time coefficients, whereas a heterogeneous

pattern can reflect the degree that one field is explained by the other field with its spatial pattern known first. It may be naturally expected that a heterogeneous correlation is weaker than a homogeneous correlation in general. Also, given that they differ significantly, these two correlations can reveal the cause and consequence between the two fields to some degree.

ACKNOWLEDGMENTS

This work was jointly supported by the 973 Program of China (2010CB950400) and the National Natural Science Foundation of China (40705021). The authors thank NCEP/NCAR for releasing reanalysis data. Valuable suggestions from the anonymous reviewers are highly appreciated.

REFERENCES

[1] Lorenz E N. The Nature and Theory of the General Circulation of the Atmosphere. Geneva: World Meteorological Organization Publication, 1967: 97-107.

[2] Yang D S, Liu Y B, Liu S K. Dynamical Meteorology (in Chinese). Beijing: Beijing Meteorological Press, 1983: 303-304.

[3] Peixoto J P, Oort A H. Physics of Climate. New York: Springer-Verlag, American Institute of Physics Press, 1992: 520.

[4] Zhang P Q, Yang S, Kousky V E. South Asian high and Asian-Pacific-American climate teleconnection. *Advances in Atmospheric Sciences*, 2005, 22(6): 915-923.

[5] Liao Q H, Tao S Y, Wang H J. Internal dynamics related to anomalies of seasonal evolution of summer circulations in East Asia during July-August. *Chinese J. Geophys.* (in Chinese), 2006, 49(1): 28-36.

[6] Zhao P, Jiang P P, Zhou X J, et al. Modeling impacts of East Asian ocean-land termal contrast on spring southwesterly winds and rainfall in eastern China. *Chinese Sci. Bull*, 2009, 54(24): 4733-4741, doi: 10.1007/s11434-009-0229-9.

[7] Lorenz E N. Available potential energy and the maintenance of the general circulation. *Tellus*, 1955, 7(2): 157-167.

[8] Dutton J A, Johnson D R. The theory of available potential energy and a variational approach to atmospheric energetics. *Advances in Geophys*, 1967, 12: 333-436.

[9] Boer G J. Zonal and eddy forms of the available potential energy equations in press coordinates. *Tellus*, 1975, 27(5): 433-442.

[10] Lorenz E N. Available energy and the maintenance of a moist circulation. *Tellus*, 1978, 30(1): 15-31.

[11] Taylor K E. Formulas for calculating available potential energy over uneven topography. *Tellus*, 1979, 31(3): 236-245.

[12] Oort A H, Asher S C, Levitus S, et al. New estimates of the available potential energy in the wold ocean. *J. Geophys. Res.*, 1989, 94(C3): 3187-3200.

[13] Shepherd T G. A unified theory of available potential energy. *Atmosphere-Ocean*, 1993, 31(1): 1-26.

[14] Winn-Nielsen A, Chen T-C. Fundamentals of Atmospheric Energetics. New York: Oxford University Press, 1993: 376.

[15] Siegmund P. The generation of available potential energy, according to Lorenz' exact and approximate equations. *Tellus*, 1994, 46A(5): 566-582.

[16] Huang R X. Available potential energy in the world's oceans. *J. Marine Research*, 2005, 63(1): 141-158.

[17] Gao L. Theoretical studies and diagnostic analyses of perturbation potential energy [Ph. D. thesis] (in Chinese). Beijing: Graduate School of the Chinese Academy of Sciences, 2006: 138.

[18] Li J P, Gao L. Theory on perturbation potential energy and its applications-concept, expression and spatio-temporal structures of perturbation potential energy. *Chinese Journal of Atmospheric Sciences* (in Chinese), 2006, 30(5): 834-848.

[19] Gao L, Li J P, Ren H L. Some characteristics of the atmosphere during an adiabatic process. *Progress in Natural Sciences* (in Chinese), 2006, 16(6): 644-648.

[20] Gao L, Li J P. Characteristics of the surface perturbation potential energy in the local atmospheric energetic efficiency. *Acta Meteorologica Sinica* (in Chinese), 2011, 69(4), 664-671.

[21] Kalnay E, Kanamitsu M, Kistler R, et al. The NCEP/NCAR 40-year reanalysis project. *Bull. Amer. Meteor. Soc.*, 1996, 77(3): 437-471.

[22] Thompson, D W J, Wallace J M. The Arctic oscillation signature in the wintertime geopotential height and temperature fields. *Geophys. Res. Lett.*, 1998, 25(9): 1297-1300.

[23] Thompson D W J, Wallace J M. Annular modes in the extratropical circulation. Part I: Month-to-month variability. *J. Climate*, 2000, 13(5): 1000-1016.

[24] Gong D Y, Wang S W. Antarctic oscillation: concept and application. *Chinese Sci. Bull.*, 1998, 43(9): 734-738.

[25] Gong D Y, Wang S W. Definition of antarctic oscillation index. *Geophys. Res. Lett.*, 1999, 26(4): 459-462.

[26] Li J P, Wang J. A modified zonal index and its physical sense. *Geophys. Res. Lett.*, 2003: 30(12): 1632, doi:10.1029/2003GL017441.

[27] Ping F, Luo Z X. The numeral simulated study of convective heat and moisture budget in the tropical. *Chinese J. Geophys.* (in Chinese), 2007, 50(5): 1351-1361.

[28] Zuo J Q, Ren H L, Li W J, et al. Intraseasonal characteristics of the water vapor transport associated with the low-frequency rainfall regimes over Southern China in summer. *Chinese J. Geophys.* (in Chinese), 2009, 52(9): 2210-2221.

[29] Gao, L, Li J P. Process in the study of atmospheric energy efficiency. *Advances in Earth Science* (in Chinese), 2007, 22(5): 486-494.